



Numerical Simulation of Rotating Vertical Bridgman Growth

S. Nouri^{1†}, P. Spiterri² and A. Ghezal¹

¹*Lmfta, usth, Bab Ezzouar, Algiers, Algeria*
²*irit, enseiht, Toulouse, France*

†*Corresponding Author Email: Nouri290676@yahoo.fr*

(Received November 9, 2014; accepted September 30, 2015)

ABSTRACT

The present work is proposed a numerical parametric study of heat and mass transfer in a rotating vertical cylinder during the solidification of a binary metallic alloy. The aim of this paper is to present an enthalpy formulation based on the fixed grid methodology for the numerical solution of convective-diffusion during the phase change in the case of the steady crucible rotation. The extended Darcy model including the time derivative and Coriolis terms was applied as momentum equation. It was found that the buoyancy driven flow and solute distribution can be affected significantly by the rotating cylinder. The problem is governed by the Navier-Stokes equations coupled with the conservation laws of energy and solute. The resulting system was discretized by the control volume method and solved by the SIMPLER algorithm proposed by Patankar. A computer code was developed and validated by comparison with previous studies. It can be observed that the forced convection introduced by rotation, dramatically changes the flow and solute distribution at the interface (liquid-mushy zone). The effect of Reynolds number on the Nusselt number, flow and solute distribution is presented and discussed.

Keywords: Vertical Solidification; Finite Volume method; Numerical analysis; Heat and mass transfer; Phase Change; Bridgman Growth.

NOMENCLATURE

Ar	aspect ratio	v	dimensionless axial velocity
g	gravitational acceleration	z	dimensionless axial coordinate
H	height of enclosure	α	thermal diffusivity
k	thermal conductivity	β_T	coefficient of thermal expansion
L	length of enclosure, m	β_s	coefficient of solutal expansion
Nu	Nusselt number	ν	kinematic viscosity
Pr	Prandtl number	ρ	density
p	dimensionless pressure		
Ra	Rayleigh number		
r	dimensionless radial coordinate		
Ste	Stefan number		
t	dimensionless time		
T	dimensionless temperature		
ΔT	temperature difference		
u	dimensionless radial velocity		

Subscripts

c	cold wall
H	hot wall
l	liquid
s	solid

1. INTRODUCTION

The study of fluid flow coupled with heat and mass transfer in rotating cylinder is of great importance due to many engineering applications in electrical, mechanical and nuclear engineering field. Several works containing such study were accomplished by many authors whose take into account various physical phenomena of heat flow and solute distribution during the phase change.

Using external forces method to control the flow and solute distribution in the melt has been experimentally and numerically investigated (Brown 1989; Muller and Ostrogorsky 1994; Lukka 2006; Stelian and Duffar 2015; Aberkane *et al.* 2015). Among the studied methods for optimization of crystal growth, the most important are the magnetic fields (Lan 2006; Inatomi *et al.* 2000; Khan *et al.* 2013) and vibration (Lan 2000). Crystal growths in a centrifuge (Lan 2001; Mueller *et al.*

1992) and under reduced gravity (Chen and Zhong 2001) have also been proposed. However, the implementation of these previous techniques is usually costly and inconvenient.

Scheel and Schulz-Dubois (1971) first introduced the acceleration crucible rotation technique (ACRT) to enhance the melt flow in vertical Bridgman crystal growth. Lan *et al.* (2000) adopted this idea for the crystal growth of ZnCdTe. They showed that the convection in the melt could be significantly suppressed by steady rotation. RoRoy *et al.* (2010) also obtained the scaling law of flow damping by the Coriolis force. He showed that the flow intensity decreased linearly with the rotation speed.

In order to reduce the unsteady and asymmetric segregation due to an arbitrary gravity orientation during crystal growth, Babalola *et al.* (2009) and Zahang (2010) proposed a possible application of using rotation. They showed by an asymptotic analysis that the rotation increased only the radial segregation. Bellmann *et al.* (2011) have been performed axisymmetric transient simulations of the vertical Bridgman growth of mc-Silicon to study the effect of the accelerated crucible rotation technique (ACRT) on the melt flow and impurity segregation. They showed that the sinusoidal ACRT rotation cycle considered in their research suppressed mixing in the melt near the center and created a limited diffusion in mass transport. H. Mei *et al.* (2013) simulated six typical ACRT modes. They adopted the standard derivation to evaluate the homogeneous level of solution concentration suggested the optimum ACRT mode and time period. M. Sekhon and S. Dost (2015) demonstrated by a numerical simulation that the potential of crucible rotation as a viable alternative to static magnetic field in inhibiting buoyancy induced flows in the Growth of SiGe.

In this paper we present for the first time a complete parametric numerical study of a solidification coupled with ACRT. The numerical model based on the Boussinesq approximation is presented. The influence of rotation on the flow, isotherms and solute distribution is analyzed via dimensionless parameters.

2. MATHEMATICAL MODEL

Consider the natural convection motion coupled with the phase change inside the cylindrical container with the top and bottom walls held at hot and cold temperatures respectively and mounted in a rotating system similar to that shown in Fig. 1. The melt is assumed incompressible and Newtonian while the flow is laminar. During phase change, three zones appear: liquid, mushy and solid zones. The mushy zone is treated as a porous medium.

Based on the Boussinesq approximation, the transport process in the melt during solidification can be described by the conservation laws for the heat and mass transfer coupled with the equations governing the momentum in the case where the angular speed Ω is constant. The governing

equations are given in dimensionless form. We distinguish:

2.1 The continuity Equation

$$\frac{1}{r} \frac{\partial(ru)}{\partial r} + \frac{\partial v}{\partial z} = 0 \quad (1)$$

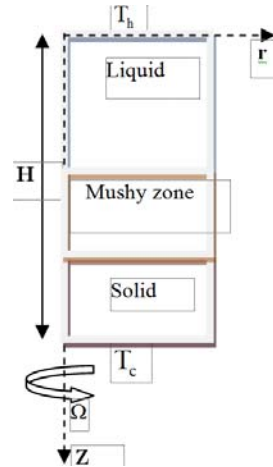


Fig. 1. Schematic of vertical Bridgman Growth.

where r and z are the respective coordinate axes in the radial and axial directions, u (respectively v) denotes the radial (respectively axial) velocity.

2.2 The Naviers – Stokes Equations

The first component u satisfy

$$\begin{aligned} \frac{\partial u}{\partial t} + u \frac{\partial u}{\partial r} + v \frac{\partial u}{\partial z} - \frac{w^2}{r} = -\frac{\partial p}{\partial r} + \frac{1}{\text{Re}} \left(\frac{1}{r} \frac{\partial}{\partial r} \left(r \frac{\partial u}{\partial r} \right) \right. \\ \left. + \frac{\partial}{\partial z} \left(\frac{\partial u}{\partial z} \right) \right) - \frac{u}{r^2} - \frac{A}{\text{Re}} u \end{aligned} \quad (2)$$

here w is the azimuthal velocity and p is the pressure. The characteristic rotational Reynolds number is the ratio between inertia and viscous forces:

$$\text{Re} = \Omega R^2 / \nu \quad (3)$$

where Ω is a characteristic rotation rate of melt.

The term A / Re describes the flow in the mushy zone. In the phase change problems, the mushy zone is assimilated to a porous medium of a porosity denoted by A (Voller and Prakash (1987)). According to Darcy's law, A is derived from the Carman-koseny (1937) equation as:

$$A = -\eta (1 - f_1)^2 / (f_1^3 + q) \quad (4)$$

with

$$f_1 = 1 - f_s \quad (5)$$

where f_s is the solid fraction, defined by:

$$f_s(T) = \begin{cases} 0 & T \geq T_{\text{Liquidus}} \\ \frac{T_{\text{Liquidus}} - T}{T_{\text{Liquidus}} - T_{\text{Solidus}}} & T_{\text{Liquidus}} > T \geq T_{\text{Solidus}} \\ 1 & T < T_{\text{Solidus}} \end{cases} \quad (11)$$

where T_{Liquidus} is the liquidus temperature at which solid formation starts and T_{Solidus} is the solidus temperature.

Remark:

In metallurgical solidification of binary alloy, the function $f_s(T)$ will depend on the nature of the solute distribution and the associated phase change equilibrium diagram. In the present work, we have chosen a simple linear form for the local solid fraction $f_s(T)$ given in the Eq. (6).

The constant η depends on the mushy zone morphology. According to Voller and Prakash 1987, η equals 1.6×10^3 . The constant q is introduced to avoid division by zero and is equal to 0.001.

The second component of the velocity v satisfies the following equation:

$$\left(\frac{\partial v}{\partial t} + u \frac{\partial v}{\partial r} + v \frac{\partial v}{\partial z} \right) = -\frac{\partial p}{\partial z} + \frac{1}{\text{Re}} \left[\frac{1}{r} \frac{\partial}{\partial r} \left(r \frac{\partial v}{\partial r} \right) + \frac{\partial}{\partial z} \left(\frac{\partial v}{\partial z} \right) \right] - \frac{A}{\text{Re}} v + \frac{\text{Ra}}{\text{Pr Re}^2} ((T-1) + N(C-1)) \quad (7)$$

The Rayleigh number Ra and buoyancy ratio N in the source terms of the momentum equation are defined as:

$$\text{Ra} \equiv (g \beta_r \Delta T R^3) / (v \alpha) \quad (8)$$

$$N \equiv \beta_c \Delta C / \beta_r \Delta T \quad (9)$$

where g is the gravitational acceleration. ΔT is the difference between the hot and cold temperature. β_r and β_c are the thermal and solutal expansion coefficients respectively. Pr is the Prandtl number defined by $\text{Pr} \equiv \rho C_p v / \lambda$.

The azimuthal velocity satisfies:

$$\left[\frac{\partial w}{\partial t} + v \frac{\partial w}{\partial z} + u \frac{\partial w}{\partial r} \right] + \frac{v \cdot w}{r} = \frac{1}{\text{Re}} \left[\frac{\partial}{\partial r} \left(r \frac{\partial w}{\partial r} \right) - \frac{w}{r^2} + \frac{\partial^2 w}{\partial z^2} \right] - \frac{A}{\text{Re}} w \quad (10)$$

2.3 The energy Equation

$$\left(\frac{\partial T}{\partial t} + u \frac{\partial T}{\partial r} + v \frac{\partial T}{\partial z} \right) = \frac{1}{\text{Pr Re}} \left[\frac{1}{r} \frac{\partial}{\partial r} \left(r \frac{\partial T}{\partial r} \right) + \frac{\partial}{\partial z} \left(\frac{\partial T}{\partial z} \right) \right] + \frac{1}{\text{Ste}} \left[\frac{\partial f_s}{\partial t} \right]$$

The Stefan number $\text{Ste} = (C_p \Delta T) / \Delta H$ scales the heat fusion ΔH released during the solidification to the sensible heat in the melt.

2.4 The Dopant Equation

The liquid concentration C_l satisfies to the following equation:

$$\left((1-f_s) \frac{\partial C_l}{\partial t} + u \frac{\partial C_l}{\partial r} + v \frac{\partial C_l}{\partial z} \right) = \frac{1}{\text{Re Sc}} \left[\frac{1}{r} \frac{\partial}{\partial r} \left(r \frac{\partial C_l}{\partial r} \right) + \frac{\partial}{\partial z} \left(\frac{\partial C_l}{\partial z} \right) \right] + (k_p - 1) C_l \frac{\partial (f_s)}{\partial t} \quad (12)$$

where the Schmidt number Sc is given by $\text{Sc} = \nu / D$ and k_p is a real number denoting the partition coefficient of the solute between the solid and liquid regions.

Equations (1)-(12) summarize the final form of the governing equations that characterize the flow, heat and mass transfer during phase change process. These equations have to be solved in a computational domain which is enclosed by solid boundaries.

2.5 Associated Boundary Conditions

For the problem of thermosolutal convection in a vertical cylindrical cavity, no slip velocities are assumed on all the boundary walls. Thus, the Dirichlet boundary conditions for velocity on all the walls can be imposed as:

$$u = v = 0 \quad (13)$$

The energy equation is solved by assuming Dirichlet temperature boundary condition on the top and bottom walls of the cavity. The lateral surface of the cylinder is assumed to be adiabatic for heat and mass transport. These conditions can be summarized as follows:

At the top ($0 < r < 1, z = H/R$):

$$w = r/R, \quad T = 1, \quad \frac{\partial c}{\partial r} = 0. \quad (14)$$

At the lateral surface ($r = 1, 0 < z < H/R$)

$$w = 1, \quad \frac{\partial T}{\partial z} = \frac{\partial c}{\partial z} = 0. \quad (15)$$

At the bottom ($0 < r < 1, z = 0$)

$$w = r/R, \quad T = 0, \quad \frac{\partial c}{\partial r} = 0. \quad (16)$$

3. NUMERICAL METHOD AND VALIDATION

The whole convection-diffusion Eqs. (1) - (16) were spatially discretized by the finite volume method. The semi-implicit time marching scheme is

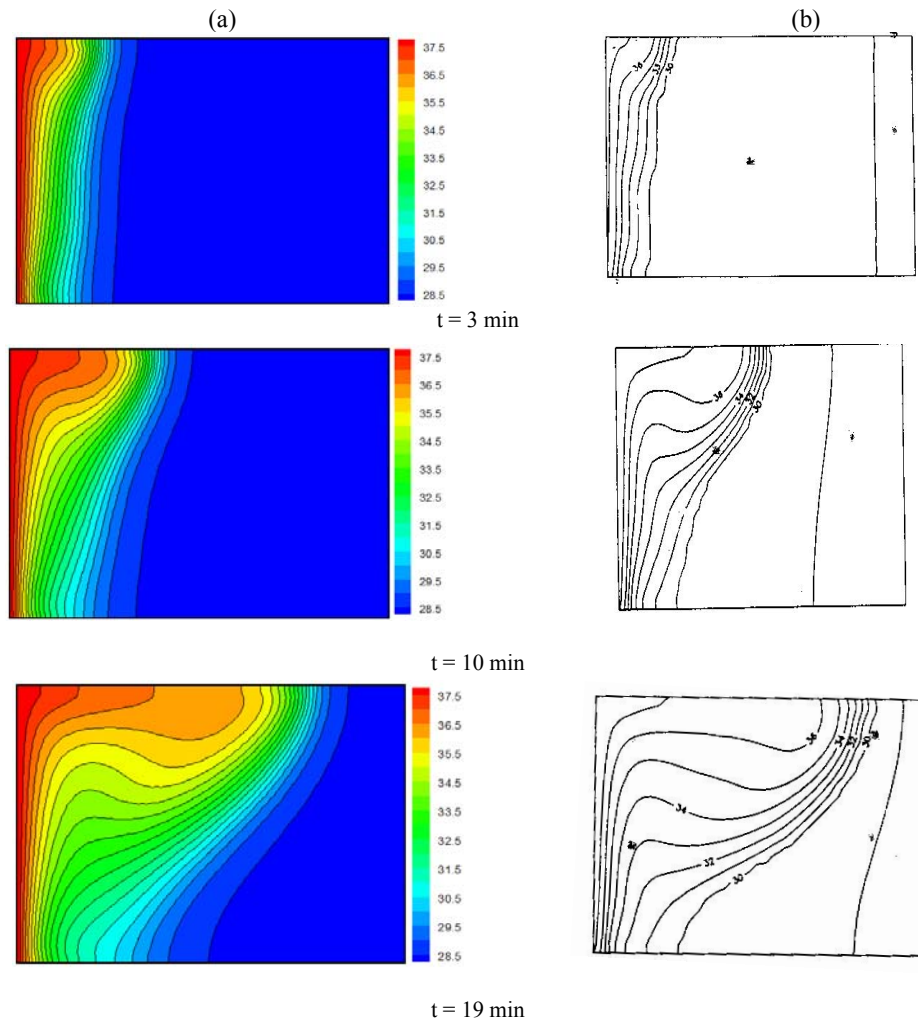


Fig. 2. Comparison of experimental and numerical data : a) Our results b) Gau and Viskanta (1986).

used for the temporal part. The coefficients of the discretized equations were expressed based on the power – law scheme which is not particularly expensive to compute and provides an extremely good representation of the exponential behavior.

The procedure used for the calculation of the flow field is the classical SIMPLER method. This procedure is well described in Patankar (1980). A line-by-line technique is applied to solve the resulting system of algebraic equations.

In the present work, an irregular exponential distribution of nodes in the radial direction in conjunction with a uniform distribution of nodes in z direction was used. The domain is meshed by 90×30 cells.

The convergence criterion was set at a maximum relative error for all dependent variables (u, v, T, C) to be less than 10^{-4} and corresponds to the satisfaction of the following inequality:

$$\text{Max} \left| \frac{\phi^{n+1} - \phi^n}{\phi^n} \right| \leq 10^{-4} \quad (17)$$

The developed code solves the unsteady state equations by introducing a non-zero time derivative (dummy time variable).

Before conducting such numerical investigations, the physical model was first used for validation compared with experimental data obtained by Gau and Viskanta (1986). Their experiment simulated is the melting of a Gallium slab heated from one side.

Initially the Gallium sample has a rectangular shape and is confined in a rigid cavity whose horizontal walls are adiabatic (dimensions of the layer, $8.89\text{cm} \times 6.35\text{cm}$). The initial temperature equals to $T_p = 28^\circ\text{C}$ below the melting temperature that is $T_m = 29.78^\circ\text{C}$.

Suddenly the left vertical wall is preheated at a temperature $T_H = 38^\circ\text{C}$ while the vertical wall at the right side is kept at $T_s = T_p$ in order to induce the

melting process in unidirectional way. Their paper reports on the role of natural convection on solid-liquid interface motion and heat transfer during melting of a pure metal (gallium) on a vertical wall.

The measurements of the position of the phase-change boundary as well as of temperature distribution were used as a qualitative indication of the natural convection flow. Numerical investigations were conducted using 2080 cells and a dimensionless time step equal to 10^{-4} ; this last value of the time step was sufficient to give accurate results. Fig. 2 shows the shape and location of the solid-liquid interface at several times during the melting process. Thus our numerical results give a good agreement compared to those of Gau and Viskanta (1986).

4. RESULTS AND DISCUSSION

The properties of the binary alloy Pb 18% Sn were obtained from Nouri *et al.* (2013). The table 1 below shows the constants and variables required for the calculations. The liquid metal, characterized by a Prandtl number equal to 0.01, is placed in a cylindrical enclosure of aspect ration (H/R=3) heated at the top wall.

Table 1 Thermo physical properties used in calculations

Quantity	Symbol	Value
Density (kg/m ³)	ρ	7.16×10^3
Dynamic viscosity (Ns/m ²)	μ	1.39×10^{-3}
Thermal conductivity (W/°C m)	λ	32.90
Specific heat (J/°C.Kg)	c_p	253.60
Thermal expansion coefficient of (C ⁻¹)	β_T	-8.75×10^{-5}
Solutal expansion coefficient	β_c	5.25×10^{-3}
Solute diffusivity(m ² /s)	D	4.50×10^{-9}
Partition coefficient	k_p	4.20
Latent heat (J/kg)	ΔH	59.150×10^3

Due to the symmetry of the geometry, boundary conditions and solution only half of the field was considered. At the initial time, the alloy is assumed to be at rest (u=v=w=0) and its temperature equal to the liquid temperature (T=1).

The dimensionless concentration equals 1 at time t=0. The crystal's rotation speed is represented by the Reynolds number $1 \leq Re \leq 10$. A sequence of simulations was performed to demonstrate the combined effect of the natural convection, segregation and forced convection which created by the melt's rotation.

Calculations in unsteady state were performed with varying the forced convection level by changing the Reynolds number and keeping the Rayleigh number and Buoyancy force ratio constant. The thermally-driven flows, represented by the stream function ψ

values, temperature field, solute distribution, pressure and angular velocity have been computed. Results are presented in dimensionless form of streamlines, isotherms, iso-concentration and iso-pressure at different Reynolds number.

Axi-symmetric simulations are performed in this paragraph in order to study the influence of the rotation on the morphological stability of the growth. The fig.3 shows that the azimuthal velocity field w, temperature profile T, pressure P, flow patterns, solute distribution and the solidification fraction development f_s are affected by the generated rotation.

The case of no rotation (w = 0), the obtained results illustrate clearly that the natural convection created by the top and bottom wall temperatures has a strong effect on the flow patterns, heat transfer and on the solute distribution at the liquid-mushy zone interface. In this case, a bi-cellular flow patterns is observed and the solute is not yet completely diffused in the mushy zone. When the rotation is considered and the Reynolds number increases, the negative flow occupies more space inside the cavity. Such reserved effect indicates that the forced convection created by the rotation becomes more effective.

When Re=1, the flow generated by the mixed convection is very low in the melt. This fact results an equality of the negative and positive flow which corresponds to an equilibrium situation. It should be noted that the flow generated by the rotation was sufficient to reverse the flow generated by the buoyancy forces. In this case of low rotation rate, the fig.3a-b shows a perfect parallelism of the isotherms and isobars. These results demonstrate that the convection created by the rotation stratifies the heat transfer and pressure field. Under these conditions, the solute distribution is extended until the mushy zone and the mass transfer mode becomes diffusive.

The applied rotation induces two opposite flow cells when Re=5, as shown in fig.3-c. The negative flow created by rotation, influences on the thermal field, solute distribution and on the solid fraction development. In this case, the cooling of the melt is prolonged and the concentration liquid is slowly transported by diffusion from the dissolution interface to the mushy zone.

At higher speed of rotation (Re ≥ 10), the positive flow develops in the middle of the negative one and the flow patterns becomes multicellular. This phenomena destabilizes more quickly the solute distribution at the interface. In this case The azimuthal velocity profil is affected.

The analysis of the rotation effect on the rate of heat transfer has been done via the average Nusselt numbers Nu_{top} and Nu_{bottom} computed respectively at the top and bottom of the cavity in cylindrical coordinates:

$$Nu_{top} = \int \frac{\partial T}{\partial Z} r dr \Big|_{z=(H/R)} \quad (18)$$

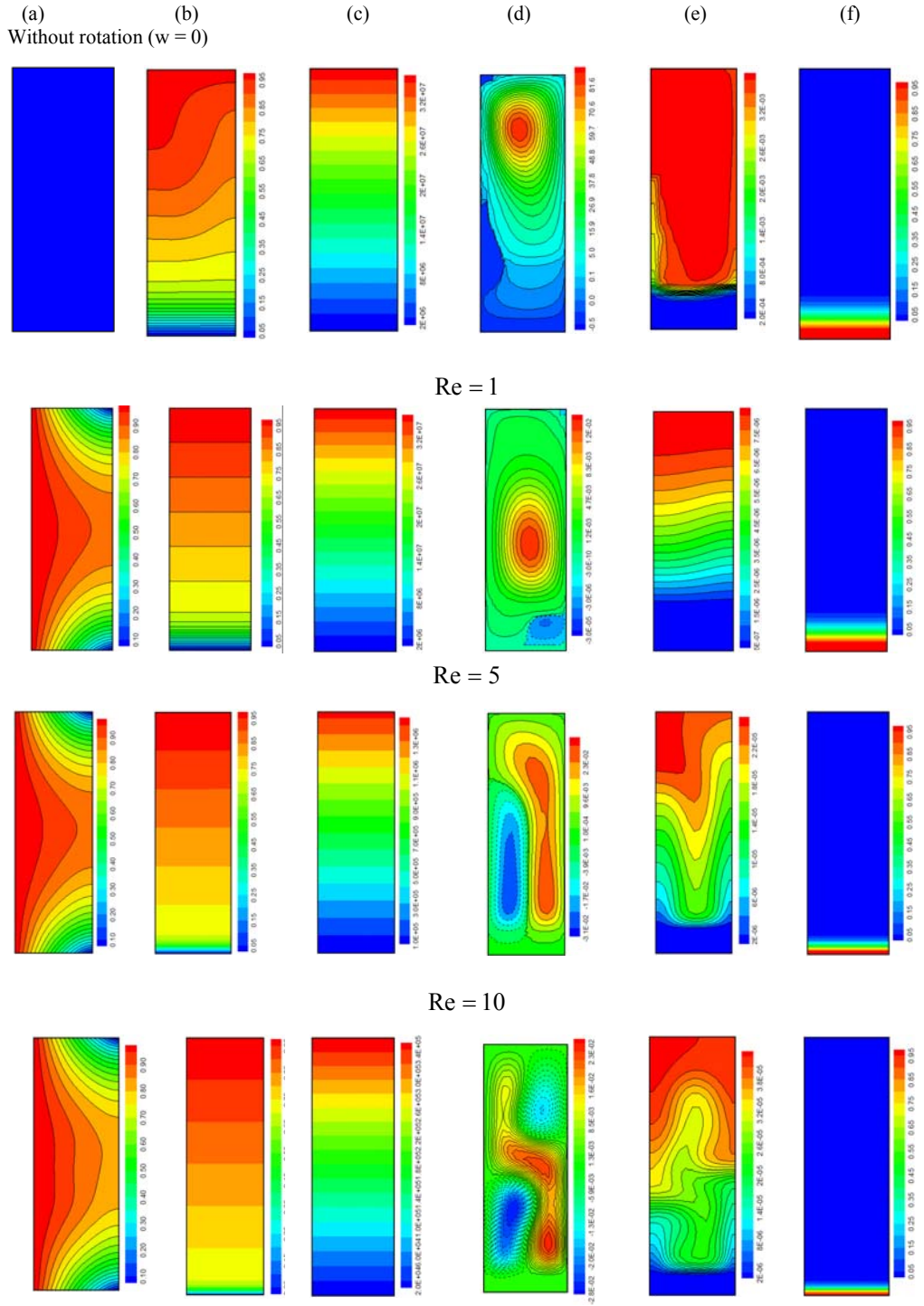


Fig. 3. Effect of Reynolds number on; a) Angular Velocity, b) Temperature Profile, c) Pressure Profile, d) Streamlines, e) Solidification Fraction.

$$\overline{Nu}_{\text{bottom}} = \int \frac{\partial T}{\partial z} r dr \Big|_{(z=0)} \quad (19)$$

In fig. 4 for Re=10, the heat transfer at the top of the cavity is more important than one at the bottom. In order to analyze better the effect of the Reynolds

number on the Nusselt number, our analysis is focused at the top of the cavity.

Fig. 5 shows the effect of the forced convection created by the rotation on the average Nusselt number $\overline{Nu}_{\text{top}}$ during the phase change. Note that

for higher values of Reynolds number, the heat transfer is very important and done in a short time. Therefore when the forced convection becomes important, the phase change becomes faster; such situation is not recommended in the crystal growth. This fact influences the flow patterns and solute distribution in the mushy zone.

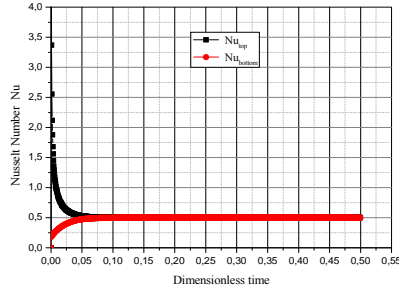


Fig. 4. Rate of heat transfer at the top and bottom of the cavity represented by the Nusselt number for $Re = 1$.

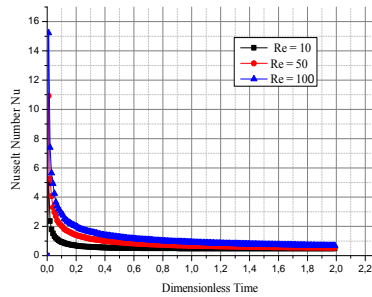


Fig. 5. Effect of the rotation on the average Nusselt number calculated at the top of cavity.

It is observed from the fig.6 that the local Nusselt number at high steady rotation rate is more important than Nusselt number calculated at low steady rotation rate. This result confirms what was found above.

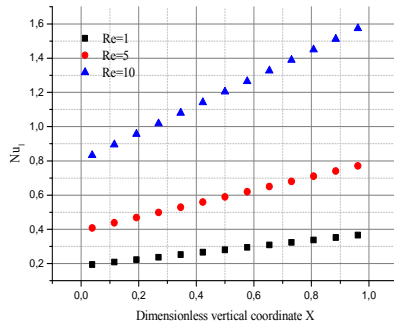


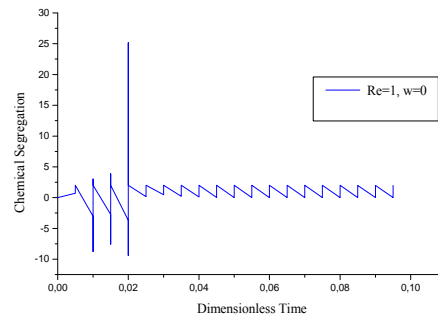
Fig. 6. Effect of the rotation on the local Nusselt number calculated at the top of cavity.

The radial segregations have been calculated by the following relationship:

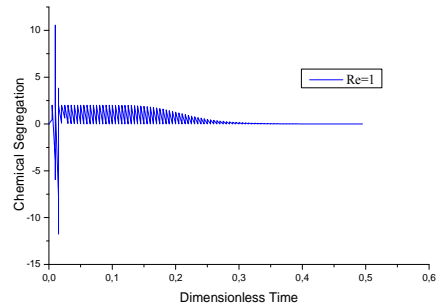
$$\delta C = (C_{\max} - C_{\min}) / C_{av} \quad (20)$$

where C_{\max} , C_{\min} and C_{av} are, respectively, the maximum, minimum and radially average interfacial concentration.

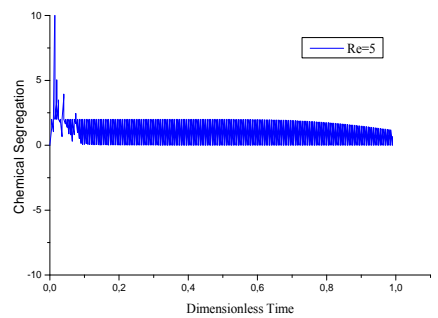
Fig. 7 illustrates that the oscillations increases vigorously with increasing of rotation speed. This means that the rotations of the crucible provoke oscillatory solute distribution and are extremely disturbing for the concentration field in the melt. When the crystal rotation rate is increased, a regular periodic oscillating solute distribution with smaller amplitude of radial segregation is observed, as in fig. 4c. In the case where no rotation is considered, the oscillations are time-dependent and irregular (fig. 4a). Those results are similar to the results found by Abbasoglu (2012).



(a)



(b)



(c)

Fig. 7. Effect of Reynolds number on radial segregation.

5. CONCLUSION

The role of steady rotation on convection and solute distribution during solidification of binary alloys was investigated via a numerical parametric study using a mathematical model based on enthalpy method. The effect of various rotation rates on macrosegregation was studied when the Reynolds number is changed. It was brought out that the application of crucible rotation does not improve the solute mixing in the melt at high rotation rates. During the crystal growth, the natural convection generated by the temperature gradient influences on the solute diffusion quality at the interface (mushy zone) and creates chemical segregations in the solid.

The crucible rotation at low Reynolds number $Re \leq 10$ generates a forced flow in the opposite direction of the thermal one. Therefore, the convection in the melt decreases and solute distribution becomes diffusive in the mushy zone. In this case, the rate of heat transfer intensity is low and the solute is moved by diffusion at the solid region. Furthermore, the use of ampoule rotation should be helpful in reducing asymmetric heat flow and solute distribution due to imperfect growth conditions.

ACKNOWLEDGMENTS

The authors gratefully acknowledge the comments and information provided by Pr Henri-Claude Boisson, Emeritus Director of Researches at the CNRS, Institut de Mécanique des Fluides IMFT of Toulouse. The authors gratefully acknowledge support provided by the Institut National Polytechnique de Toulouse and the Institut de Recherche en Informatique de Toulouse during the early stages of Miss Nouri.

REFERENCES

- Abbasoglu, S. (2012). Three-dimensional numerical simulation of crystal and crucible rotations during Czochralski growth of Ge_xSi_{1-x} single crystals. *Turk J Elec Eng & Comp Sci* 20, 2-9.
- Aberkane, S., M. Ihdene, M. Mordes and A. Ghezal (2015). Axial magnetic field effect on Taylor-Couette flow, *Journal of applied fluid mechanics* 8, 255-264.
- Babalola, O., A. Bolotnikov and M. Groza (2009). Study of Te inclusions in CdMnTe crystals for nuclear detector application, *International Journal of Crystal Growth* 311, 3702-3707.
- Bellmann, M. P., E. A. Meese and L. Arnberg (2011). Effect of accelerated crucible rotation on the segregation of impurities in vertical Bridgman growth of multi-crystalline silicon, *Journal of Crystal Growth* 318, 239-243.
- Brown, R. (1988). Theory of transport processes in single crystal growth from the melt, *AIChE J* 34, 881-991.
- Carman, P. (1937). *Trans. inst. Chem. engrs* 15, 150-166.
- Chen, N., X. Zhong and L. Lin (2001). Comparison of field effect transistor characteristics between space-grown and earth-grown gallium arsenide single crystal substrates. *Applied Physics* 78(4), 478-479.
- Gau, C., R. Viskanta (1986). Melting and solidification of a pure metal on a vertical wall, *Journal of Heat Transfer* 108, 174-181.
- Inatomi, Y., A. Kato, K. Horiuchi, K. Takada and K. Kuribayashi (2000). Scaling Analysis of Semiconductor Crystal Growth from the Liquid Phase in an Axis Static Magnetic Field, *Material Transactions* 41, 1026-1033.
- Khan, M., R. Ali and A. Shahzad (2013). MHD Falkner-Skan flow with mixed convection and convective boundary conditions, *Walailak Journal of Science and Technology (WJST)* 10(5), 517-529.
- Lan, C. W. (2000). Effects of axial vibration on vertical zone-melting processing, *International Journal of Heat Mass Transfer* 43, 1987-1997.
- Lan, C. W. (2001). Effects of centrifugal acceleration on the flows and segregation in vertical Bridgman crystal growth with steady ampoule rotation, *International Journal of Crystal Growth* 229, 595-600.
- Lan, C., M. Liang and J. Chian (2000). Influence of ampoule rotation on three-dimensional convection and segregation in Bridgman crystal growth under imperfect growth conditions, *International Journal of Crystal Growth* 212, 340-351.
- Lukka, P., T. Lampen and L. Wandlan (2006). Test Beam Results of a proton irradiated Czochralski Silicon Strip detector, *Nuclear instruments and Methods in Physics Research A* 568, 72-77.
- Lan W. (2006). Recent progress of crystal growth modelling and growth control, *Chemical Engineering Science* 59, 1437-1457.
- Mei, H., Z. Zeng, Z. Qiu, L. Li, L. Yao, H. Mizuseki and Y. Kawazae (2013). Numerical simulation of crucible rotation in high-temperature solution growth method using a Fourier-Legendre spectral element method, *International of Heat and Mass Transfer* 64, 882-891.
- Mingwen, C., J. Xiaojin, Z. Yahohon, Q. Ping and Z. wang (2013). The Effect of the Shear Flow on Particle Growth in the Undercooled Melt, *journal of 17th International Conference on Crystal Growth and Epitaxy - ICCGE-17*
- Mueller, G., G. Neumann and W. Weber (1992). The growth of homogeneous semiconductor crystals in a centrifuge by the stabilizing influence of the Coriolis force, *International Journal of Crystal Growth* 119, 8-23.

- Muller, G. and A. Ostrogorsky (1994). Growth Mechanisms and Dynamics, *Handbook, North-Holland*.
- Nouri, S., M. Benzeghiba and A. Ghezal (2013). Effect of Steady Ampoule on Radial Dopant Segregation in Vertical Bridgman Growth, *International book Series Advanced Structured Materials Springer 41*, 250 .
- Patankar, S. (1980). Numerical heat transfer and fluid flow. *Mc Graw Hill Book Company* .
- Roroy, U. and S. Weiler (2010). Study of 2 in diameter CdZnTe by THM technique, *International Journal of Crystal Growth* 312, 2840-2845.
- Scheel, H. (1971). Accelerated crucible rotation; a novel stirring technique in a high temperature solution, *International Journal of Crystal Growth* 13(14), 560-565.
- Sekhon, M. and S. Dost (2015). Numerical examination of the effect of steady crucible rotation in the liquid phase diffusion growth of SiGe, *Journal of Crystal Growth* 430, 63-70.
- Stelian, C. and T. Duffar (2015). Influence of rotating magnetic fields on THM growth of CdznTe crystals under microgravity and grown conditions. *International Journal of Crystal Growth* 429, 19-26.
- Voller, V. and K. Prakash (1987). A fixed grid numerical modeling methodology for convection-diffusion mushy region phase-change problems, *International Journal of Heat and Mass Transfer* 30, 1709-1719.
- Zahang, J., W. Jie, L. Wang and L. Luan (2000). Twins in CdMnTe single crystals grown by Bridgman method, *Crystal Research and Technology* 45, 7-12.